Corresponding author: V.V. Atuchin
Institute of Semiconductor Physics, Novosibirsk 630090, Russia
Fax: +7 (383) 3332771
E-mail: atuchin@isp.nsc.ru

Structural and spectroscopic properties of self-activated monoclinic molybdate $BaSm_2(MoO_4)_4$

V.V.Atuchin[1,2,3,4,5], A.S. Aleksandrovsky[6,7], M.S. Molokeev[8,9], A.S. Krylov[10], A.S. Oreshonkov[10,11], Di Zhou[12,13]

[1]Laboratory of Optical Materials and Structures, Institute of Semiconductor Physics, SB RAS, Novosibirsk 630090, Russia

[2]Functional Electronics Laboratory, Tomsk State University, Tomsk 634050, Russia

[3]Laboratory of Semiconductor and Dielectric Materials, Novosibirsk State University, Novosibirsk 630090, Russia

[4]Institute of Chemistry, Tyumen State University, Tyumen 625003, Russia

[5]Laboratory of Single Crystal Growth, South Ural State University, Chelyabinsk 454080, Russia

[6]Laboratory of Coherent Optics, Kirensky Institute of Physics, Federal Research Center KSC SB RAS, Krasnoyarsk 660036, Russia

[7]Laboratory for Nonlinear Optics and Spectroscopy, Siberian Federal University, Krasnoyarsk 660041, Russia

[8]Laboratory of Crystal Physics, Kirensky Institute of Physics, SB RAS, Krasnoyarsk 660036, Russia

[9]Department of Physics, Far Eastern State Transport University, Khabarovsk 680021, Russia

[10]Laboratory of Molecular Spectroscopy, Kirensky Institute of Physics, Federal Research Center KSC SB RAS, Krasnoyarsk 660036, Russia

[11]Department of Photonics and Laser Technologies, Siberian Federal University, Krasnoyarsk 660079, Russia

[12]Electronic Materials Research Laboratory, Key Laboratory of the Ministry of Education & International Center for Dielectric Research, Xi'an Jiaotong University, Xi'an 710049, Shaanxi, China

[13]Materials Science and Engineering, University of Sheffield, Sheffield, S1 3JD, UK

Abstract

Crystal structure of new monoclinic molybdate $BaSm_2(MoO_4)_4$ is refined in monoclinic unit cell *C*2/*m* with cell parameters a=5.29448 Å, b=12.7232 Å, c=19.3907 Å, beta=91.2812 º, V= 1305.89 $Å^3$. Crystal structure consists of SmO_8 square antiprism joined with each other by edges forming 2D layer perpendicular to c-axis. MoO_4 tetrahedra join to SmO_8 by nodes and also participate in formation of layer, and Ba ions are located between these layers. Lattice dynamics is theoretically calculated on the base of crystal structure data. Raman spectra are recorded and analyzed in comparison with theoretical calculations. Discrepancy between the experimental and calculated Raman frequencies does not exceed 2 cm^{-1} for the most of Raman lines. Luminescence spectra of Sm ions, which positioned in the lowest local symmetry site C_1, strongly differ from those detected for another molybdate crystal, β-$RbSm(MoO_4)_2$, with C_2 local symmetry. $^4G_{5/2} \rightarrow {}^6H_{9/2}$ band is dominating in the luminescence of $BaSm_2(MoO_4)_4$.

Keywords:

1. Introduction

Presently, materials based on crystalline structure of various rare-earth-containing molybdates are under extensive study in connection with a number of applications including solid-state lighting [1-7], upconverting phosphors ([9,10] and references therein), energy storage [11], microwave electronics [12-14], catalysis [15,16], laser and stimulated Raman scattering media [17,18], etc. Crystal structure of multicationic molybdates can exhibit a number of structural features such as polymorphism, incommensurate modulation, structure-inferred vacancies, ionic occupation disorder. as well as the possibility of controlling the local environment of rare-earth ions by varying the nomenclature and content of additional ions [19-22]. The latter is of importance for the optical properties of rare-earth ions such as distribution of absorption cross-sections and luminescence intensities between different bands as well as the shapes of these bands themselves, due to strong influence of crystal field on the probabilities of *f* - *f* transitions and energy structure of crystal-field-split sublevels. Another important factor influencing optical properties of rare-earth ions in crystalline matrices is the interaction between electronic excitations and vibrational modes; this interaction influences the radiativeless relaxation processes that decrease the luminescence intensities and change the distribution of populations of excited states. Finally, different matrices may favor dipole-dipole energy transfer between ions to a larger or smaller extent, that, in the particular, influences concentration quenching of luminescence. For instance, monoclinic α-$Eu_2(MoO_4)_3$ crystal was found to be exhibit rather strong Eu ion luminescence indicating weaker concentration quenching than in other highly concentrated crystals [23,24].

In the present paper, the crystal structure, luminescence and Raman spectra of new monoclinic molybdate crystal $BaSm_2(MoO_4)_4$ are investigated. Earlier, similar crystal structure was reported for $BaNd_2(MoO_4)_4$ [25], and, recently, the microwave properties of $BaSm_2(MoO_4)_4$ ceramics were elucidated [12], however, the structural and spectroscopic properties of this crystal remain unknown..

2. Experimental

The $BaSm_2(MoO_4)_4$ ceramic samples were prepared via solid state reaction method using $BaCO_3$, Sm_2O_3 and MoO_3 (>99%) as initial materials. The calcination temperature was 700 °C and the sintering temperature is 960 °C. More details can be found in our previous work. [12] Microstructures of ceramic were observed on the as-fired surface with scanning electron microscopy (SEM) (JSM-6460, JEOL, Tokyo, Japan).

The powder diffraction data of BaSm2(MoO4)4 for Rietveld analysis were collected at room temperature with a Bruker D8 ADVANCE powder diffractometer (Cu Kα radiation) and linear VANTEC detector. The step size of 2θ was 0.016° and the counting time was 2 s per step. The 2θ range of 5-70º was measured with 0.6mm divergence slit, but 2θ range of 70-140º was measured with 2mm divergence slit. Larger slits allow noticeably increase in intensity of high-angle peaks without loss of resolution because the high-angle peaks are broad enough to be not affected by bigger divergence beam. The esd's $\sigma(I_i)$ of all points on patterns were calculated using intensities I_i: $\sigma(I_i)=I_i^{1/2}$. The intensities and obtained esd's were further normalized: $I_{i\ norm} = I_i \times 0.6/(\text{slit width})$, $\sigma_{norm}(I_i) = \sigma(I_i) \times 0.6/(\text{slit width})$, taking into account actual value of divergence slit width which was used to measure each particular intensity I_i, and saved in xye-type file. So transformed powder pattern has usual view in whole 2θ range of 5-140º, but all high-angle points have small esd values.

Luminescence spectra were recorded under the excitation at 355 nm using DPSS frequency-tripled Nd:YAG LaserCompact LCS-DTL-374QT laser and LOMO DFS-24 spectrometer. The unpolarized Raman spectra were collected in a backscattering geometry using a triple monochromator Horiba Jobin Yvon T64000 Raman spectrometer operating in subtractive mode. The spectral resolution for the recorded Stokes side Raman spectra was set to ~4 cm^{-1} (this resolution was reached by using gratings with 1800 grooves/mm and 100 mm slits). The microscope system based on Olympus BX41 microscope with an Olympus 50^x objective lens f = 0.8 mm with NA=0.75 numerical aperture provides a focal spot diameter of about 2 μm on the sample [26,27]. Single-mode argon 514 nm from a Spectra-Physics Stabilite 2017 Ar^+ laser of 3

mW on the sample was used as excitation light source. The intensity of the laser light was adjusted to avoid sample heating. Positions and widths of spectral lines were obtained by least square fitting of the experimental data to the Lorentzian equation [28]:

$$I_L = \frac{A}{1+\left(\frac{x-\omega}{\Gamma}\right)^2}$$

where A – amplitude, ω – wavenumber, Γ – full width at half height, and x – actual coordinate (wavenumber).

3. Results and discussions

The XRD pattern recorded from the $BaSm_2(MoO_4)_4$ sample is shown in Fig. 1. The Rietveld refinement of $BaSm_2(MoO_4)_4$ XRD data was performed by using TOPAS 4.2 [29] which accounts esd's of each point by special weight scheme. All peaks were indexed by monoclinic cell (*C*2/*c*) with parameters close to those of $BaNd_2(MoO_4)_4$ [25] and, therefore, the crystal structure of $BaNd_2(MoO_4)_4$was taken as a starting model for Rietveld refinement. However, nonstandard space group *B*2/*b* used in Ref. 25 was transformed into standard setting *C*2/*c*, and all coordinates of atoms were transformed accordingly. The site of Nd ion was occupied by Sm ion. In order to reduce number of refined parameters, only one thermal parameter was refined for all O atoms. The refinement was stable and gives low R-factors (Table 1, Fig.1). The coordinates of atoms and main bond lengths are summarized in Tables S1 and S2, respectively.

The crystal structure consists of SmO_8 square antiprisms joined with each other by edges forming 2D layers perpendicular to *c*-axis, as shown in Figure 2. The MoO_4 tetrahedra join to SmO_8 by nodes and also participate in formation of the layers and Ba^{2+} ions are located between these layers. Namely, such layered crystal structure leads to interesting effect of changing cell parameters due to $Sm^{3+} \rightarrow Nd^{3+}$ ion replacement. As far as ion radii IR(Nd^{3+}, CN = 8) = 1.109 Å is bigger that IR(Sm^3, CN = 8) = 1.079 Å, the cell volume of $BaNd_2(MoO_4)_4$ (V = 1323.22 $Å^3$) [25] is predictably bigger than cell volume of $BaSm_2(MoO_4)_4$ (V = 1305.89 (2) $Å^3$). But only *a* and *b* cell parameters

are responsible for this cell volume changing: δa = 0.64 %, δb = 0.63 %, δc = 0.03 %. Cell parameter *c* stays almost invariable, but relative changes of *a*, *b* parameters are noticeable and similar in magnitude. This is because the substitution $Sm^{3+} \rightarrow Nd^{3+}$ leads to enlargement of 2D layer only. However, the distance between the layers is governed by the size of Ba^{2+} ion (Figure 2). Further comparison of cell parameters $BaSm_2(MoO_4)_4$ and $BaYb_2(MoO_4)_4$ [http://dx.doi.org/10.1515/znb-1996-0116] also show similar behavior: δa = 2.13 %, δb = 2.01 %, δc = 0.21 %. Therefore, the cell parameter deformations can be predictable and controlled by different ions A, Re in the formula $ARe_2(MoO_4)_4$.

Further details of the crystal structure may be obtained from Fachinformationszentrum Karlsruhe, 76344 Eggenstein-Leopoldshafen, Germany (fax: (+49)7247-808-666; E-mail: crystdata@fiz-karlsruhe.de; http://www.fiz-karlsruhe.de/request_for_deposited_data.html on quoting the deposition number CSD-??????.

The SEM pattern is shown in Fig. 3. As it is evident, the sample bulk is formed by closely packed well faceted plate-like microcrystals with length of 2-5 μm and ~1 μm in thickness. The temperature of 960 °C is in the range of active sublimation of molybdenum oxide in the air environment and this process stimulates the material exchange during the synthesis of molybdates that results in the formatiuon of microcrystals with equilibrial shapes and atomically flat facets [23,30,31].

The Raman spectrum recorded from $BaSm_2(MoO_4)_4$ powder is shown in Fig. 4. About 40 narrow Raman lines were revealed by the experimental spectrum fitting, and the complete set of Raman lines found in $BaSm_2(MoO_4)_4$ is shown in Table 4. The Raman spectrum of $BaSm_2(MoO_4)_4$ can be divided into two parts with a wide empty gap of 500-700 cm^{-1} that is commonly observed in molybdates with MoO_4 tetrahedra [32-40]. The extended spectra with component decomposition in the low and high wavenumber ranges are shown in Figures 1S and 2S. In the range of stretching vibrations of MoO_n polyhedra (n = 4 or 6, 720-940 cm^{-1}), a lot of lines were observed. The most

intensive line is detected at 950.2 cm^{-1}. The Raman spectra obtained under excitation at 514.5 and 488 nm are shown comparatively in Figure 3S.

Vibrational representation for the monoclinic phase at Brillouin zone center is:

$$\Gamma_{vibr} = 34A_g + 34A_u + 34B_g + 35B_u;$$

Acoustic and optic modes: $\Gamma_{acoustic} = A_u + 2B_u$, $\Gamma_{optic} = 34A_g + 33A_u + 34B_g + 33B_u$;

Infrared and Raman active modes:$\Gamma_{raman} = 34A_g + 34B_g$,$\Gamma_{infrared} = 33A_u + 33B_u$.

To calculate the $BaSm_2(MoO_4)_4$ vibrational spectrum, the program package LADY was used [41]. The atomic vibration values were obtained using the simplified version of the Born-Karman model [42]. Within this model, only the pair-wise interactions and bond-stretching force constants *F*are considered and the model implies that *F* depends on r_{ij} (interatomic distance) and the $F(r_{ij})$ functions are the same for all atom pairs: $F(r_{ij}) = \lambda\exp(-r_{ij}/\rho)$, where λ and ρ are the parameters characterizing selected pair interaction. To find the model parameters, the special optimization program was written and tested for several compounds [10, 23, 43-56]. The crystal lattice stability conditions were taken into account. The parameters finally obtained for $BaSm_2(MoO_4)_4$ are shown in Table 1S.

The calculations show that 52 Raman-active modes are possible in the range of <500 cm^{-1}. Besides, 1 mode around 500 cm^{-1} and 16 Raman-active modes should appear in the range of >700 cm^{-1}. This is in agreement with the selection rules and calculated parameters of 69 possible Raman active modes are summarized in Table 4 in comparison with experimental results.

The strong high-wavenumber band at 950.2 cm^{-1} is assigned to the Mo2 – O7 bond stretching vibration (Mo–O bond with shortest length in $BaSm_2(MoO_4)_4$), as shown in Fig. 5(a). The next one strong peak at 925 cm^{-1} is a Mo1 – O2 bond stretching vibration. The band at 890 cm^{-1}corresponds to the O1 – Mo1 – O3 antisymmetric stretching vibration depicted in Fig. 5(b). The strong band at 854 cm^{-1} is a symmetric stretching vibration of O1, O2 and O3 atoms towards Mo1, as shown in

Fig. 5(c). The relatively weak bands at 802 and 753 cm^{-1} are ν_3 vibrations [57] of Mo2 and Mo1 tetrahedra correspondingly. Because Mo1 – O5 bond length is longer than other bonds in Mo1 tetrahedra by more than 0.13Å, wavenumber of the corresponding vibration descended in the region of 713 cm^{-1} (Fig. 5(d)). According to the lattice dynamics simulation, vibration of oxygen bridge between Mo1 tetrahedra (Fig. 5(e)) should appear in Raman spectra in the region about 500 cm^{-1}, and this vibration probably can be observed in Raman spectra at low temperature [58]. The Raman lines over the 270-420 cm^{-1} range related to MoO_4 bending modes. Generally, the frequency of ν_4 vibration should be above that of ν_2 vibration [57], and our calculation results are in agreement with this relation. The region of 200-260 cm–1 is a region of rotational vibrations of the tetrahedral group. As to the low wavenumber range of 40-200 cm^{-1}, this region contain external vibrations of MoO_4 units, translational and mixed with MoO_4 vibrations of Ba and Sm ions.

Luminescence spectra of $BaSm_2(MoO_4)_4$ were recorded under the excitation at the wavelengths 355, 488 and 514.5 nm. Radiation at 355 nm (28200 cm^{-1}) falls into the absorption bands at the transitions from Sm^{3+} ground state $^6H_{5/2}$ to a number of closely spaced high-lying states, most probably, to $^4H_{7/2}$. Radiation at 488 nm (20500 cm^{-1}) excites another group of closely lying excited states, most probably, $^4I_{9/2}$. Radiation at 514.5 nm (19430 cm^{-1}) is not in good resonance with samarium absorption bands. Fig. 5 depicts 355 nm excited luminescence of $BaSm_2(MoO_4)_4$ ceramic sample (thick red line) in comparison with another molybdate, β-$RbSm(MoO_4)_2$ (blue thin line), used as the reference sample [59].

As shown in Fig. 6, luminescence of $BaSm_2(MoO_4)_4$ ceramic is found to be weaker than that of β-$RbSm(MoO_4)_2$ powder, and recording of its spectrum required larger slit width. There is strong difference between the distributions of luminescence bands' intensities in $BaSm_2(MoO_4)_4$ and β-$RbSm(MoO_4)_2$. Three main luminescent bands are observed for $BaSm_2(MoO_4)_4$, all of them starting from $^4G_{5/2}$ state. The maximum luminescence band of $BaSm_2(MoO_4)_4$ corresponds to the $^4G_{5/2} \rightarrow {}^6H_{9/2}$ transition, while in reference sample we observed absolute domination of $^4G_{5/2} \rightarrow {}^6H_{5/2}$ transition terminating at the ground state of samarium ion. Evidently, the difference noted above is

connected with the different local symmetry of samarium in the crystal structure under study and in the reference $RbSm(MoO_4)_2$ structure. In both crystals, samarium ion is surrounded by 8 neighboring oxygen ions. However, its local symmetry in $BaSm_2(MoO_4)_4$ is C_1 while in the reference crystal the local symmetry is C_2 and can be associated with strongly distorted cubic antiprism. That strong distortion is the origin of specific spectral distribution of luminescence in the reference crystal $RbSm(MoO_4)_2$ [59]. The local environment of samarium in $BaSm_2(MoO_4)_4$ can hardly be associated with any kind of distortion of a regular polyhedron (Fig. 7).

On the other hand, spectral distribution of luminescence in $BaSm_2(MoO_4)_4$ is somehow closer to a traditional one, for instance in most of Sm^{3+}-bearing glasses. Local environment of samarium in glasses is formed mainly by chemical properties of samarium itself; this local environment is the result of minimum of interaction potential energy that is attained during the time of glassy structure formation. Judd-Ofelt parameters of samarium in different glassy matrices are rather close to each other [60]. Typically, in glasses, the $^4G_{5/2} \rightarrow {}^6H_{7/2}$ transition dominates in the luminescence while $^4G_{5/2} \rightarrow {}^6H_{5/2}$ and $^4G_{5/2} \rightarrow {}^6H_{9/2}$ bands are smaller. In $BaSm_2(MoO_4)_4$, $^4G_{5/2} \rightarrow {}^6H_{5/2}$ transition, in difference with glasses, is the smallest, while $^4G_{5/2} \rightarrow {}^6H_{9/2}$ is the strongest one, and $^4G_{5/2} \rightarrow {}^6H_{9/2}$ is slightly weaker but of comparable amplitude. $^4G_{5/2} \rightarrow {}^6H_{11/2}$ transition, being typically the smallest of all in glasses, is also observed in $BaSm_2(MoO_4)_4$ (not shown in Fig. 6) but its magnitude is close to noise level, while in the reference crystal it was not detected at all. Potential energy minimum attained under the crystal structure formation is deeper than in case of glassy state and it is governed by the interactions within the crystal unit cell, i.e. at larger distances than in glass. The peculiarities described above indicate that the role of crystal structure in the formation of Sm^{3+} local environment is very high in the reference crystal structure, however, in the $BaSm_2(MoO_4)_4$ crystal the influence of matrix is also noticeable in comparison with glassy ones. Another feature that can be noted is the absence of luminescent bands from states higher than $^4G_{5/2}$ in $BaSm_2(MoO_4)_4$. These bands are well seen in the reference crystal, that indicates the stronger radiativeless relaxation from higher-lying states to $^4G_{5/2}$ in $BaSm_2(MoO_4)_4$ than that in β-$RbSm(MoO_4)_2$. One of these states is

$^4I_{9/2}$ that produces well detectable luminescence in the blue range in β-$RbSm(MoO_4)_2$ when excited at 355 nm. This level, however, can be directly excited by 488 nm radiation. We have tested this excitation channel and have found that luminescence spectrum under 488 nm excitation is in close agreement with that excited at 355 nm. Main difference is the increase of intensity of weak band above 700 nm due to $^4G_{5/2} \rightarrow {}^6H_{11/2}$ transition and minor redistribution of intensities of crystal-field-split components within $^4G_{5/2} \rightarrow {}^6H_{9/2}$ band, while $^4G_{5/2} \rightarrow {}^6H_{5/2}$ and $^4G_{5/2} \rightarrow {}^6H_{7/2}$ bands are almost untouched by the excitation wavelength change. The observed differences indicate fine variation of population distribution between $^4G_{5/2}$ components at 488 nm excitation with respect to 355 nm excitation.

4. Conclusions

In the present work, the binary molybdate $BaSm_2(MoO_4)_4$ was successfully synthesized by the ceramic method. The crystal structure and spectroscopic characteristics of the crystal were exhibited for the first time. The structure is layered and the interlayer distance is controlled by the size of Ba^{2+} ion. This specific geometry provides highly anisotropic behavior of the cell parameters on the substitution of Sm^{3+} by other rare earth ions. As an example, the comparison of the presently-known cell parameters in monoclinic $BaSm_2(MoO_4)_4$, $BaNd_2(MoO_4)_4$ and $BaYb_2(MoO_4)_4$ possesses noticeable variation of *a* and *b* parameters and a very small variation of *c* parameter. This specific structural feature may be an indicator of high anisotropy of physical properties, including thermal, optical and dielectric parameters. Testing of the effects is the challenge for nearest future, when the single crystals of the molybdates from this family will be available.

Acknowledgements

This work was supported by the National Natural Science Foundation of China (U1632146). The reported study was funded by RFBR according to the research project 16-52-48010, 17-52-

53031 and 16-32-00351 mol_a. Also, the work was supported by (Act 211) the Government of the Russian Federation, contract 02.A03.21.0011 , by Project № 0356-2015-0412 of SB RAS Program№II.2P, and by the Ministry of Education and Science of the Russian Federation (4.1346.2017/PP).

References

1. Pinglu Shi, Zhiguo Xia, M.S. Molokeev, V.V. Atuchin, Crystal chemistry and luminescence properties of red-emitting $CsGd_{1-x}Eu_x(MoO_4)_2$ solid-solution phosphors, Dalton Trans. 43 (2014) 9669-9676.
2. Wentao Zhang, Junfeng Li, Yulong Wang, Jianping Long, Kehui Qiu, Synthesis and luminescence properties of $NaLa(MoO4)_{2-x}AG_x:Eu^{3+}$ (AG = SO_4^{2-}, BO_3^{3-}) red phosphors for white light emitting diodes, J. Alloys Compd. 635 (2015) 16-20.
3. Huajuan Deng, Ze Zhao, Jing Wang, Zhoufei Hei, Mengxue Li, Hyeon MiNoh, Jung HyunJeong, RuijinYu, Photoluminescence properties of a new orange–red emitting Sm^{3+}-doped $Y_2Mo_4O_{15}$ phosphor, J. Solid State Chem. 228 (2015) 110–116.
4. M. Janulevicius, J. Grigorjevaite, G. Merkininkaite, S. Sakirzanovas, A. Katelnikovas, Luminescence and luminescence quenching of $Eu_2Mo_4O_{15}$, J. Lumin. 179 (2016) 35–39.
5. Yun Liu, Jinyang Li Haoqiang Zuo, Xiaolei Shi, Suiyan Ma, Minzhu Zhao, Synthesis and luminescent properties of $KLa_{1-x-y}(MoO_4)_{2-z}(WO_4)_z:xEu^{3+},yDy^{3+}$ phosphors for WLEDs, J. Mater. Sci.: Mater. Electron. 27 (2016) 9470–9475.
6. Jing Li, Li Chen, Jiahua Zhang, Zhendong Hao, Yongshi Luo, Ligong Zhang, Photoluminescence properties of a novel red-emitting phosphor Eu^{3+} activated scandium molybdate for white light emitting diodes, Mat. Res. Bull. 83 (2016) 290-293.
7. Dong-ni Wu, Xin-yong Gong, Rui-rui Cui, Chao-yong Deng, Luminescence properties of Ca^{2+} and Si^{4+} co-doped strontium molybdate red phosphors for white LEDs, J. Mater. Sci.: Mater. Electron. 27 (2016) 9661–9667.
8. V. Mahalingam, M. Syed Gulam Ambia, J. Thirumalai, R. Krishnan, R. Chandramohan, Spectroscopic investigations of Sm^{3+} doped $Ca_{0.5}La(MoO_4)_2$phosphor for solid state lighting applications, J. Mater. Sci.: Mater. Electron. 28 (2017) 2838–2845.

9. Chang Sung Lim, V. Atuchin, A. Aleksandrovsky, M. Molokeev, A. Oreshonkov, Microwave sol–gel synthesis of $CaGd_2(MoO_4)_4:Er^{3+}/Yb^{3+}$ phosphors and their upconversion photoluminescence properties, J. Am. Ceram. Soc. 98 (2015) 3223-3230.
10. Chang Sung Lim, A. S. Aleksandrovsky, M. S. Molokeev, A. S. Oreshonkov, D. A. Ikonnikov, V. V. Atuchin, Triple molybdate scheelite-type upconversion phosphor $NaCaLa(MoO_4)_3:Er^{3+}/Yb^{3+}$ structural and spectroscopic properties, Dalton Trans. 45 (2016) 15541-15551.
11. Li-Qiang Mai, Fan Yang, Yun-Long Zhao, Xu Xu, Lin Xu, & Yan-Zhu Luo, Hierarchical $MnMoO_4/CoMoO_4$ heterostructured nanowires with enhanced supercapacitor performance, Nature Comm. 2:381 (2011) 2-5.
12. Di Zhou, Li-Xia Pang, Jing Guo, Ying Wu, Gao-Qun Zhang, Wei Dai, Hong Wang, Xi Yao, New microwave dielectric ceramics $BaLn_2(MoO_4)_4$ (Ln = Nd and Sm) with low loss, J. Am. Ceram. Soc. 94 (2011) 2800-2803.
13. Wen-Bo Li, Hai-Hong Xi, Di Zhou, Microwave dielectric properties of temperature-stable $BaLn_2(MoO_4)_4$-TiO_2 (Ln = Ce, Nd, and Sm) ceramics, J. Elect. Mater. 44 (11) (2015) 4250-4254.
14. Li-Xia Pang, Wei-Guo Liu, Di Zhou, Zhen-Xing Yue, Phase evolution and microwave dielectric properties of $(Bi_{1-x}Ln_x)_2MoO_6$ (Ln = Nd and La, $x \leq 0.3$) ceramics, Ceram. Int. 42 (2016) 17243-17247.
15. P. Hongda Li, Wenjun Li, Shaonan Gu, Fangzhi Wang, Hualei Zhou, Xintong Liu, Chaojun Ren, Enhancement of photocatalytic activity in Tb/Eu co-doped Bi_2MoO_6: the synergistic effect of Tb-Eu redox cycles, RSC Adv. 6 (2016) 48089-48098.
16. F. Namvar, F. Beshkar, M. Salavati‐Niasari, S. Bagheri, Morphology-controlled synthesis, characterization and photocatalytic property of hierarchical flower-like $Dy_2Mo_3O_9$ nanostructures, J. Mater. Sci.: Mater. Electron. (2017) DOI 10.1007/s10854-017-6799-4.

17. A. V. Lebedev, S. A. Avanesov, Barium–bismuth molybdate – a novel promising material for stimulated Raman scattering, Mater. Lett. 161 (2015) 661-664.
18. Yang Zhang, Hengjiang Cong, Huaidong Jiang, Jing Li, Jiyang Wang, Flux growth, structure, and physical characterization of new disordered laser crystal $LiNd(MoO_4)_2$, J. Cryst. Growth 423 (2015) 1–8.
19. A.M. Abakumov, V,A, Morozov, A.A. Tsirlin, J. Verbeeck, J. Hadermann, Cation ordering and flexibility of the BO_4^{2-} tetrahedra in incommensurately modulated $CaEu_2(BO_4)_4$ (B = Mo, W) scheelites, Inorg. Chem. 53 (2014) 9407-9415.
20. G.D. Tsyrenova, E.T. Pavlova, S.F. Solodovnikov, N.N. Popova, T.Y. Kardash, S.Y. Stefanovich, I.A. Gudkova, Z.A. Solodovnikova, B.I. Lazoryak, New ferroelastic $K_2Sr(MoO_4)_2$: synthesis, phase transitions, crystal and domain structure, ionic conductivity, J. Solid State Chem. 237 (2016) 64-71.
21. Chang Sung Lim, V.V. Atuchin, A.S. Aleksandrovsky, M.S. Molokeev, A.S. Oreshonkov, Incommensurately modulated structure and spectroscopic properties of $CaGd_2(MoO_4)_3$:Ho^{3+}/Yb^{3+} phosphors for up-conversion applications, J. Alloys Compd. 695 (2017) 737-746.
22. S.F. Solodovnikov, V.V. Atuchin, Z.A. Solodovnikova, O.Y. Khyzhun, M.I. Danilenko, D.P. Pishchur, P.E. Plusnin, A.M. Pugachev, T.A. Gavrilova, A.P. Yeliseeyev, Ali H. Reshak, Zeyad A. Alahmed, Nadir F. Habubi, Synthesis, structural, thermal, and electronic properties of palmierite-related double molybdate α-$Cs_2Pb(MoO_4)_2$, Inorg. Chem. 56 (6) (2017) 3276-3286.
23. V. V. Atuchin, A. S. Aleksandrovsky, O. D. Chimitova, T. A. Gavrilova, A. S. Krylov, M. S. Molokeev, A. S. Oreshonkov, B. G. Bazarov, J. G. Bazarova, Synthesis and spectroscopic properties of monoclinic α-$Eu_2(MoO_4)_3$, J. Phys. Chem. C 118 (2014) 15404–15411.
24. Ali H. Reshak, Z.A. Alahmed, J. Bila, V.V. Atuchin, B.G. Bazarov, O.D. Chimitova, M.S. Molokeev, I.P. Prosvirin, A.P. Yelisseyev, Exploration of the electronic structure of monoclinic

α-$Eu_2(MoO_4)_3$: DFT-based study and X-ray photoelectron spectroscopy, J. Phys. Chem. C 120 (2016) 10559-10568.

25. I. I. Kiseleva, M. I. Sirota, R. P.Ozerov, T. P.Balakireva, A. A.Majer, Double barium lanthanide molibdates $BaLn_2(MoO_4)_4$. Kristallografiya, 24(6), 1979, 1277-1279.
26. A.V. Malakhovskii, T.V. Kutsak, A.L. Sukharev, A.S. Aleksandrovsky, A.S. Krylov, I.A. Gudim, M.S. Molokeev, Spectroscopic properties of $ErAl_3(BO_3)_4$ single crystals, Chem. Phys. 428 (2014) 137-143.
27. A.S. Krylov, S.V. Goryainov, N.M. Laptash, A.N. Vtyurin, S.V. Melnikova, S.N. Krylova, Influence of the molecular groups ordering on structural phase transitions in $(NH_4)_2WO_2F_4$, Cryst. Growth Des. 14 (1) (2014) 374-380.
28. Peter A. Jansson, Deconvolution with applications in spectroscopy – Academic Press, 1984.
29. Bruker AXS TOPAS V4: General profile and structure analysis software for powder diffraction data. – User's Manual. Bruker AXS, Karlsruhe, Germany. 2008.
30. I.B. Troitskaia, T.A. Gavrilova, S.A. Gromilov, D.V. Sheglov, V.V. Atuchin, R.S. Vemuri, C.V. Ramana, Growth and structural properties of α-MoO_3 (010) microplates with atomically flat surface, Mater. Sci. Eng. B 174 (1-3) (2010) 159-163.
31. V.V. Atuchin, T.A. Gavrilova, T.I. Grigorieva, N.V. Kuratieva, K.A. Okotrub, N.V. Pervukhina, N.V. Surovtsev, Sublimation growth and vibrational microspectrometry of α-MoO_3 single crystals, J. Cryst. Growth 318 (2011) 987-990.
32. M. Buijs, G. Blasse, Nonresonant energy transfer in a system with two different rare-earth sites: β′-$Gd_2(MoO_4)_3$:Eu^{3+} and β′-$Eu_2(MoO_4)_3$, Phys. Rev. B 34 (12) (1986) 8815-8821.
33. J. Hanuza, L. Macalik, K. Hermanowicz, Vibrational properties of $KLn(MoO_4)_2$ crystals for light rare earth ions from lanthanum to terbium, J. Mol. Struct. 319 (1994) 17-30.
34. L. Macalik, Comparison of the spectroscopic and crystallographic data of Tm^{3+} in the different hosts: $KLn(MoO_4)_2$ where Ln = Y, La, Lu and M = Mo, W, J. Alloys Compd. 341 (2002) 226-232.

35. V. Dmitriev, V. Sinitsyn, R. Dilanian, D. Machon, A. Kuznetsov, E. Ponyatovsky, G. Lucazeau, H.P. Weber, In situ pressure-induced solid-state amorphization in $Sm_2(MoO_4)_3$, $Eu_2(MoO_4)_3$ and $Gd_2(MoO_4)_3$ crystals: chemical decomposition scenario, J. Phys. Chem. Solids 64 (2003) 307-312.
36. V.V. Atuchin, O.D. Chimitova, T.A. Gavrilova, M.S. Molokeev, Sung-Jin Kim, N.V. Surovtsev, B.G. Bazarov, Synthesis, structural and vibrational properties of microcrystalline $RbNd(MoO_4)_2$, J. Cryst. Growth 318 (2011) 683-686.
37. V.V. Atuchin, V.G. Grossman, S.V. Adichtchev, N.V. Surovtsev, T.A. Gavrilova, B.G. Bazarov, Structural and vibrational properties of microcrystalline $TlM(MoO_4)_2$ (M = Nd, Pr) molybdates, Opt. Mater. 34 (2012) 812-816.
38. M. Maczka, A.G. Souza Filho, W. Paraguassu, P.T.C. Freire, J. Mendes Filho, J. Hanuza, Pressure-induced structural phase transitions and amorphozation in selected molybdates and tungstates, Prog. Mater. Sci. 57 (2012) 1335-1381.
39. V.V. Atuchin, O.D. Chimitova, S.V. Adichtchev, B.G. Bazarov, T.A. Gavrilova, M.S. Molokeev, N.V. Surovtsev, Zh.G. Bazarova, Synthesis, structural and vibrational properties of microcrystalline β-$RbSm(MoO_4)_2$, Mater. Lett. 106 (2013) 26-29.
40. V.V. Atuchin, A.S. Aleksandrovsky, O.D. Chimitova, A.S. Krylov, M.S. Molokeev, B.G. Bazarov, J.G. Bazarova, Zhiguo Xia, Synthesis and spectroscopic properties of multiferroic β′-$Tb_2(MoO_4)_3$, Opt. Mater. 36 (2014) 1631-1635.
41. M.B. Smirnov, V.Yu. Kazimirov, LADY: software for lattice dynamics simulations. (JINR communications), E 14-2001-159, 2001.
42. M. Smirnov, R. Baddour-Hadjean, Li intercalation in TiO_2 anatase: Raman spectroscopy and lattice dynamic studies, J. Chem. Phys.121 (2004) 2348-2355.
43. A.N. Vtyurin, A.S. Krylov, S.N. Krylova, S.V. Goryainov, V.N. Voronov, A.S. Oreshonkov, Hydrostatic pressure-induced phase transitions in Rb_2KInF_6 and Rb_2KScF_6 crystals: Raman spectra and lattice dynamics simulations, Ferroelectrics 440 (2012)100-104.

44. A.S. Krylov, A.N. Vtyurin, A.S. Oreshonkov, V.N. Voronov, S.N. Krylova, Structural transformations in a single-crystal Rb_2NaYF_6: Raman scattering study, J. Raman Spectr., 44 (2013) 763-769.

45. Y.V. Gerasimova, A.S. Oreshonkov, A.N. Vtyurin, A.A. Ivanenko, L.I. Isaenko, A.A. Ershov, E.I. Pogoreltsev,Infrared absorption investigation of the role of octahedral groups upon the phase transition in the $Rb_2KMoO_3F_3$ crystal, Phys. Solid State 55 (2013) 2331-2334.

46. Zhiguo Xia, M.S. Molokeev, A.S. Oreshonkov, V.V. Atuchin, Ru-Shi Liu, Cheng Dong, Crystal and local structure refinement in $Ca_2Al_3O_6F$ explored by X-ray diffraction and Raman spectroscopy, Phys. Chem. Chem. Phys. 16 (2014) 5952-5957.

47. A.A. Savina, V.V. Atuchin, S.F. Solodovnikov, Z.A. Solodovnikova, A.S. Krylov, E.A. Maximovskiy, M.S. Molokeev, A.S Oreshonkov, A.M. Pugachev, E.G. Khaikina, Synthesis, structural and spectroscopic properties of acentric triple molybdate $Cs_2NaBi(MoO_4)_3$, J. Solid State Chem. 225 (2015) 53–58.

48. C.S. Lim, A.S. Aleksandrovsky, M.S. Molokeev, A.S. Oreshonkov, V.V. Atuchin, The modulated structure and frequency upconversion properties of $CaLa_2(MoO_4)_4$:Ho^{3+}/Yb^{3+}phosphors prepared by microwave synthesis, Phys. Chem. Chem. Phys. 17 (2015) 19278-19287.

49. C.S. Lim, A. Aleksandrovsky, M. Molokeev, A. Oreshonkov, V. Atuchin, Microwave sol–gel synthesis and upconversion photoluminescence properties of $CaGd_2(WO_4)_4$:Er^{3+}/Yb^{3+} phosphors with incommensurately modulated structure, J. Solid State Chem. 228 (2015) 160-166.

50. A.S. Oreshonkov, J.V. Gerasimova, A.A. Ershov, A.S. Krylov, K.A. Shaykhutdinov, A.N. Vtyrin, M.S. Molokeev, K.Y. Terent'ev, N.V. Mihashenok, Raman spectra and phase composition of $MnGeO_3$ crystals, J. Raman Spectr. 47 (2016) 531–536.

51. A.S. Oreshonkov, A.S. Krylov, N.P. Shestakov, V.N. Voronov, A.A. Ershov, E.A. Strikina, A.N. Vtyurin, Vibrational spectra of NdF_3 crystal, Ferroelectrics 501 (2016) 15-19.

52. E.A. Strikina, A.S. Krylov, A.S. Oreshonkov, A.N. Vtyurin, Raman scattering study of δ-BiB_3O_6 crystal, Ferroelectrics 501 (2016) 26-31.
53. E.A. Strikina, A.S. Krylov, A.S. Oreshonkov, A.N. Vtyurin, O.A. Maximova, Anisotropic crystal of the δ-BiB_3O_6 investigated by vibrational spectroscopy, IOP Conf. Ser.: Mater. Sci. Eng. 155 (2016) 012029.
54. A.S. Krylov, M.S. Molokeev, S.V. Misyul, S.N. Krylova, A.S. Oreshonkov, A.A. Ivanenko, V.A. Zykova, Y.N. Ivanov, A.A. Sukhovsky, V.N. Voronov, I.N. Safonov, A.N. Vtyurin, Crystal structure and phase transitions of layered perovskite-like $CsScF_4$ crystal, CrystEngComm, 18 (2016) 8472-8486.
55. Y.V. Gerasimova, A.S. Oreshonkov, O.B. Romanova, A.A. Ivanenko, A.S. Krylov, Spectr. Lett. 50 (2017) 55-58.
56. Yu.V. Gerasimova, A.S. Oreshonkov, N.M. Laptash, A.N. Vtyurin, A.S. Krylov, N.P. Shestakov, A.A. Ershov, A.G. Kocharova, Raman and infrared spectroscopic characterization of gadolinium-doped manganese sulfide, Spectrochim. Acta A 176 (2017) 106-113.
57. K. Nakamoto, Infrared and Raman Spectra of Inorganic and Coordination Compounds, 6th edn. Wiley, New York etc., 2009.
58. J. Hanuza, E.B. Burgina, G.A. Osipov, E.N. Yurchenko, The low temperature spectra and normal coordinate analysis of $KY(MoO_4)_2$ crystal, J. Mol. Struct. 158 (1987) 141-152.
59. V. V. Atuchin, A. S. Aleksandrovsky, O. D. Chimitova, Cheng-Peng Diao, T. A. Gavrilova, V. G. Kesler, M. S. Molokeev, A. S. Krylov, B. G. Bazarov, G. Bazarova, Zheshuai Lin, Electronic structure of β-$RbSm(MoO_4)_2$ and chemical bonding in molybdates, Dalton Trans. 44 (2016) 1805-1815.
60. R. Van Deun, K. Binnemans, C Gorler-Walrand, J.L.Adam, Spectroscopic properties of trivalent samarium ions in glasses. Proc. SPIE, 3622 (1999) 175 – 181.

Table 1. Main parameters of processing and refinement of the $BaSm_2(MoO_4)_4$sample

Compound	$BaSm_2(MoO_4)_4$
Sp.Gr.	*C*2/*c*
a, Å	5.29448 (5)
b, Å	12.7232 (1)
c, Å	19.3907 (2)
β, º	91.2812 (6)
V, Å^3	1305.89 (2)
Z	4
2θ-interval, º	5-140
R_{wp}, %	2.26
R_p, %	1.95
R_{exp}, %	1.36
χ^2	1.66
R_B, %	1.01

Table 2. Calculated wavenumber versus experimental relative magnitude (*I*), wavenumber and full width at half maximum (FWHM) of the Raman lines

ω, cm^{-1} (calc.)		*I*, (exp.)	ω, cm^{-1} (exp.)	Γ (FWHM), cm^{-1}
A_g	B_g			
950.1	946.4	100	950.2	3.2
925.1	924.3	2.4 29.7	929.1 925.3	1.9 3.4
886.0	889.8	12.8 3.4	890.4 883.0	4.7 6.1
847.6 820.4	847.0 820.4	71.4 1.5	854.6 840.8	8.3 30.3
802.7	802.6	3.8	799.8	9.8
750.5	750.7	9.2	753.0	9.5
704.8	705.7	4.1 0.3	713.3 702.5	11.0 11.2
499.7				
418.4		1.2	417.7	7.6
	407.3	2.8	406.1	8.1
381.6	380.4	5.5 1.7	394.9 383.4	10.9 8.62
365.3 354.5	364.2 355.7	5.3	361.4	6.5
339.4	343.2	10.8	345.0	11.8
320.0	319.5	28.0 2.9	322.1 313.0	9.7 6.1
299.0 297.4	306.6 294.6	1.3	297.7	10.0
288.3	285.9	1.0	280.7	9.7
271.2	274.6 263.9	1.1	269.0	9.1
253.8		0.03	252.6	7.4
	253.4	0.3	244.5	9.4
227.9		2.5	225.6	10.3
206.8	213.9	0.01	211.6	2.6
195.1	199.6	3.2	181.9	6.3
172.2	166.3	5.1	161.1	5.1
153.9	155.6	1.5	155.9	4.7
142.0	141.8	18.9	145.9	4.8
139.1		8.5	139.0	4.8
	134.2	3.0	132.8	3.5
123.2	122.8	4.1	127.3	4.1
120.4	114.1	3.4	118.2	3.4
	113.3	3.0	113.7	3.5
103.4		16.5	108.7	2.7
	102.2	2.9	101.5	3.8
93.9	89.6	0.6	94.8	1.2
85.7	81.5	9.9	83.8	3.0
73.6	78.1 67.6	3.8	73.8	2.5
48.7	48.2	10.6	49.0	2.4

Captions

Fig 1. Difference Rietveld plot of $BaSm_2(MoO_4)_4$.

Fig. 2. Crystal structure of $BaSm_2(MoO_4)_4$. The unit cell is outlined. The lone atoms of Sm, Mo and O are omitted for clarity.

Fig. 3. SEM pattern of the $BaSm_2(MoO_4)_4$ microcrystals.

Fig. 4. Raman spectra of $BaSm_2(MoO_4)_4$.

Fig. 5. Calculated vibration modes of the MoO_4 tetrahedrons in $BaSm_2(MoO_4)_4$. a) *Ag* 950.1 cm^{-1}, b) *Ag* 886.0 cm^{-1}, c) *Ag* 847.6 cm^{-1}, d) Ag 704.8 cm^{-1}, e) Ag 499.6 cm^{-1}.

Fig. 6. Luminescence spectra of $BaSm_2(MoO_4)_4$ (thick red) and β-$RbSm(MoO_4)_2$ (thin blue) excited at 355 nm.

Fig. 7. Local environment of Sm^{3+} ion in $BaSm_2(MoO_4)_4$ (left) and β-$RbSm(MoO_4)_2$ (right) crystal structures.

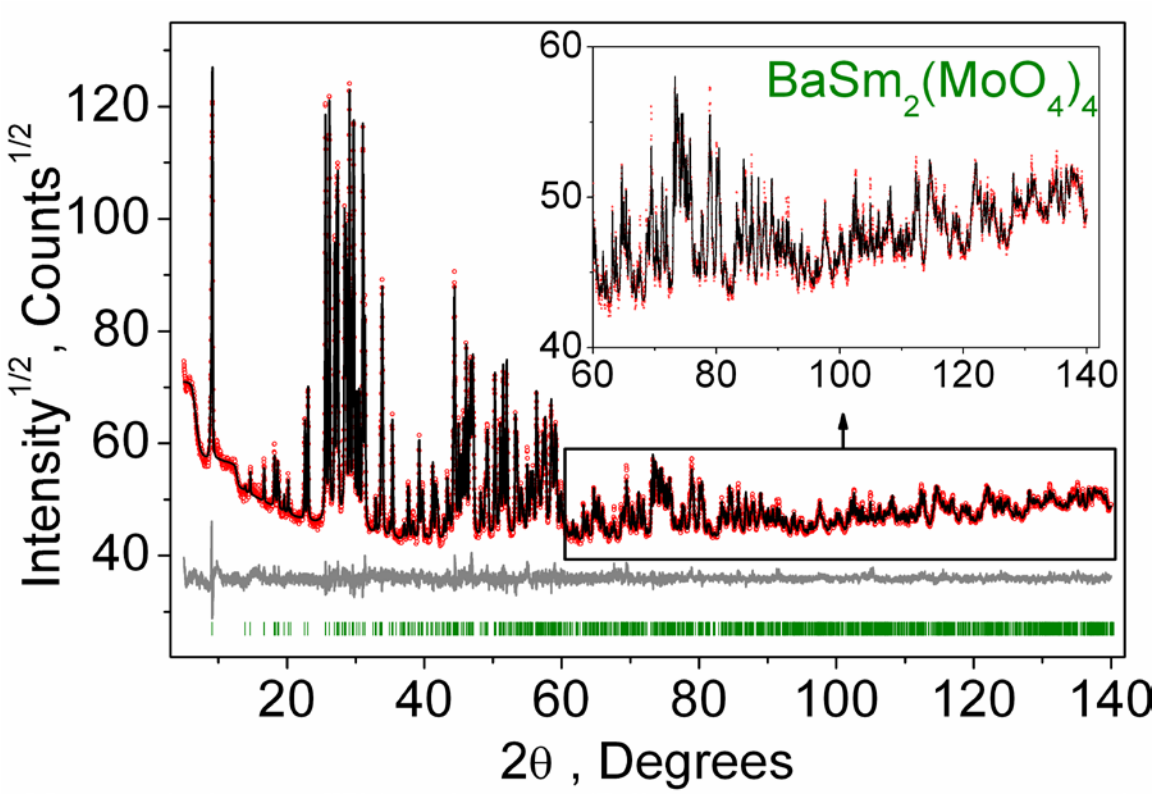

Figure 1.

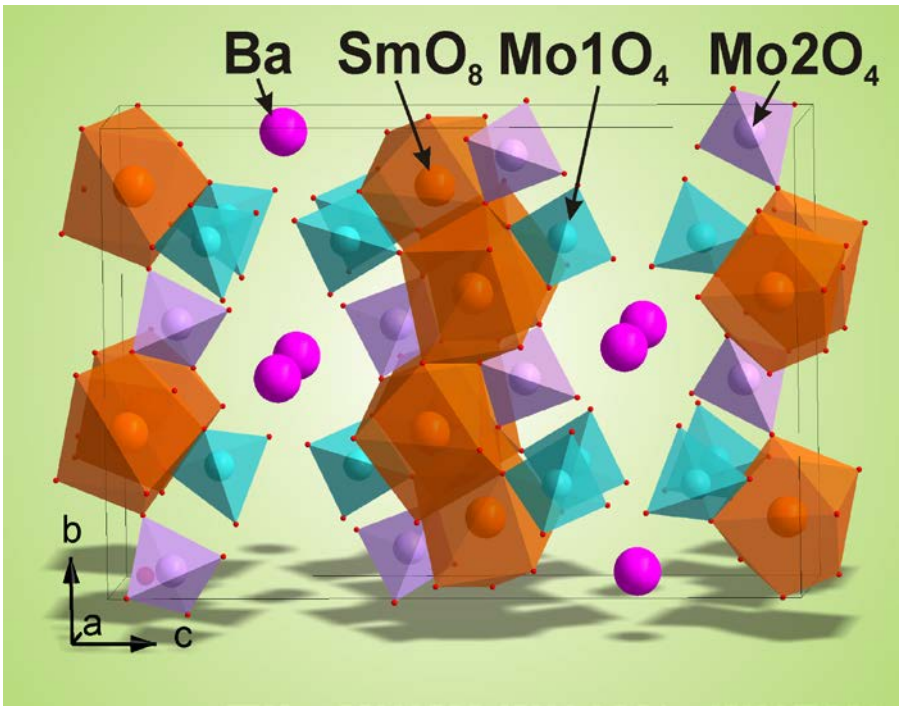

Figure 2.

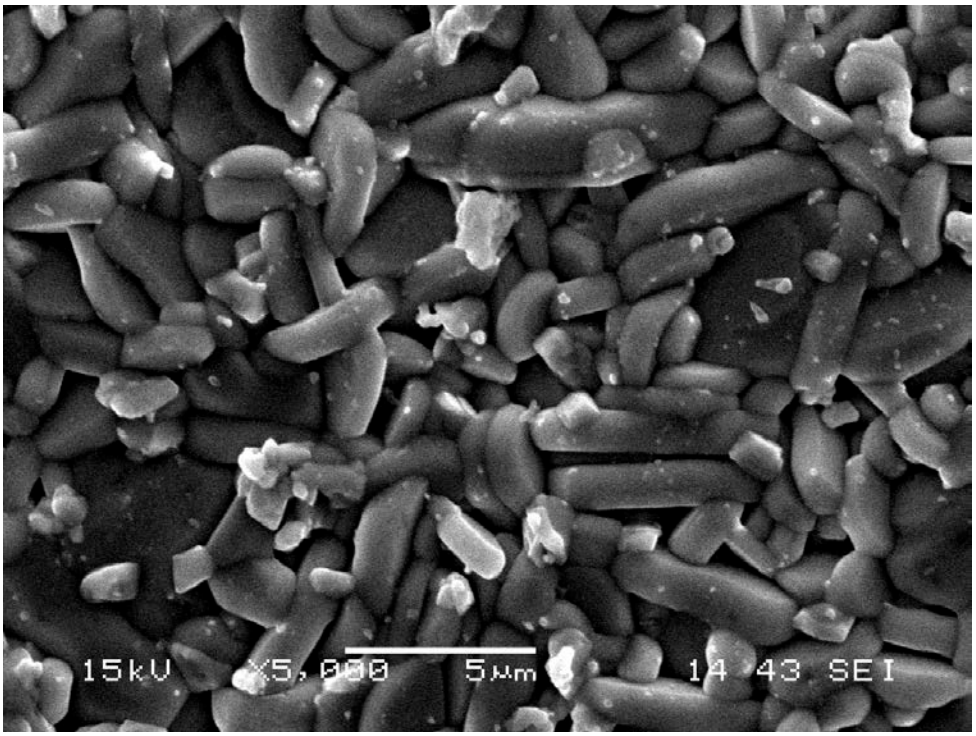

Figure 3.

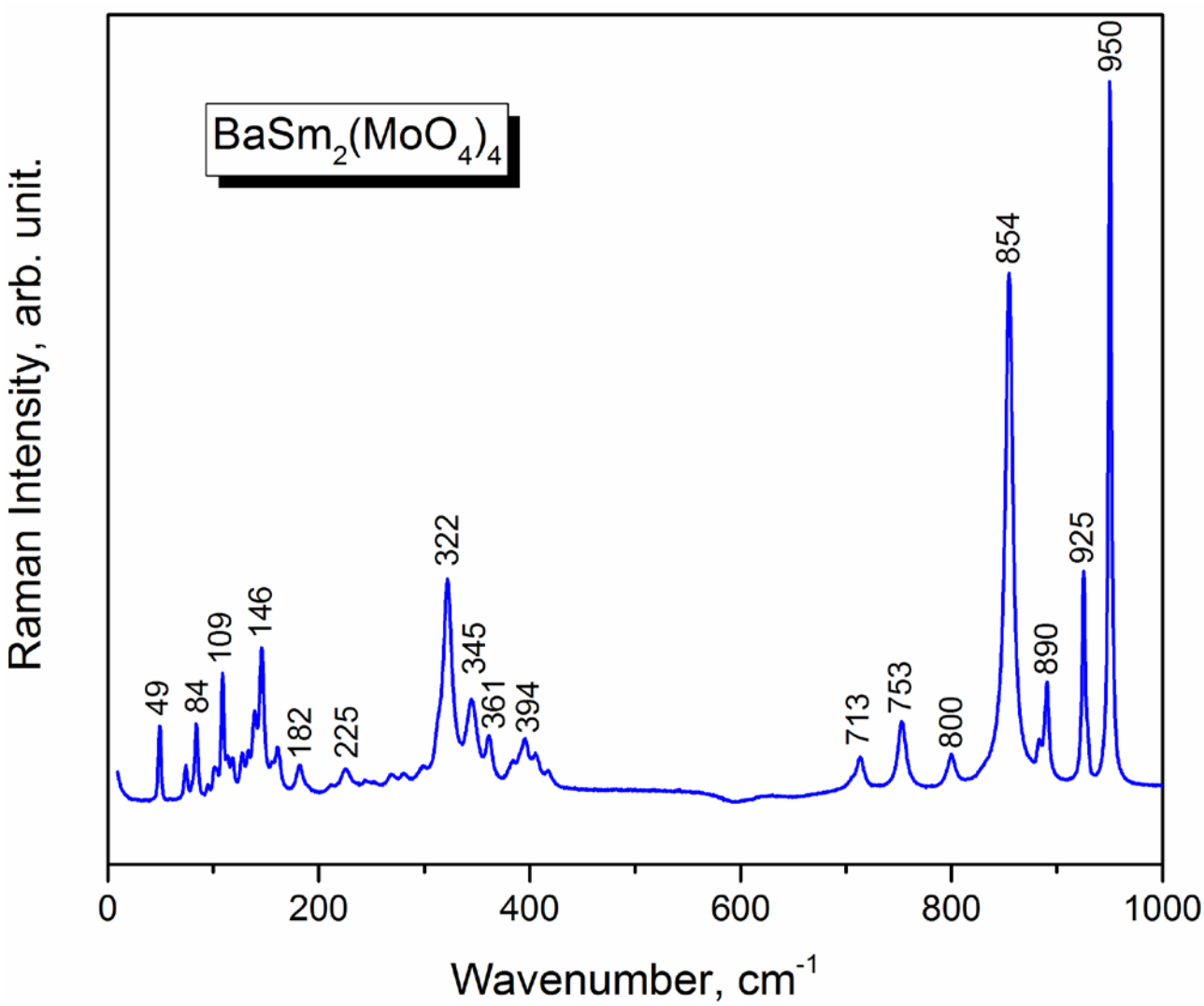
BaSm2(MoO4)4
Raman Intensity, arb. unit.
Wavenumber, cm-1
0
200
400
600
800
1000
49
84
109
146
182
225
322
345
361
394
713
753
800
854
890
925
950

Figure 4.

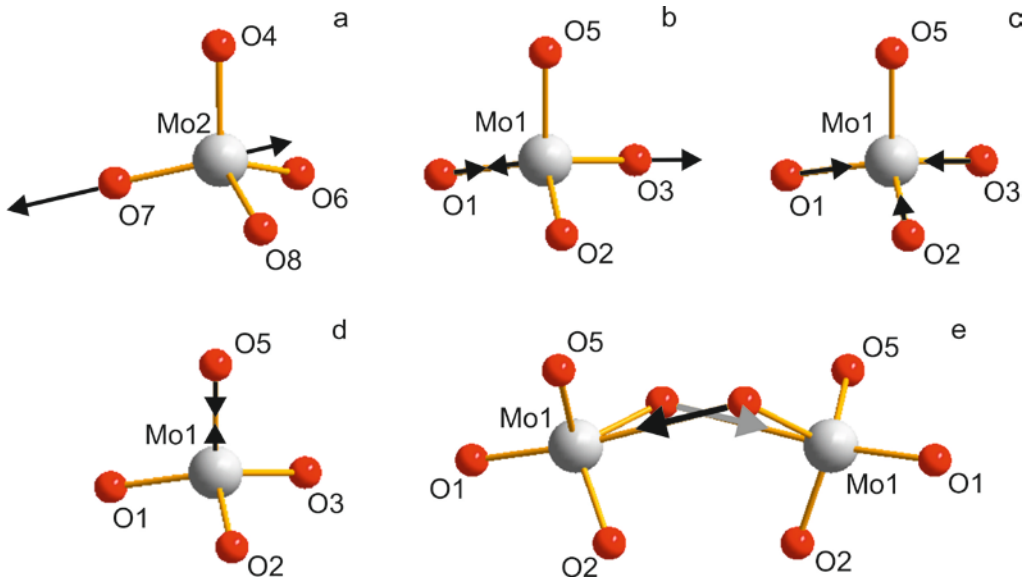
a
O4
Mo2
O7
O6
O8
b
O5
Mo1
O1
O3
O2
c
O5
Mo1
O1
O3
O2
d
O5
Mo1
O1
O3
O2
e
O5
Mo1
O1
O2
O5
Mo1
O1
O2

Figure 5.

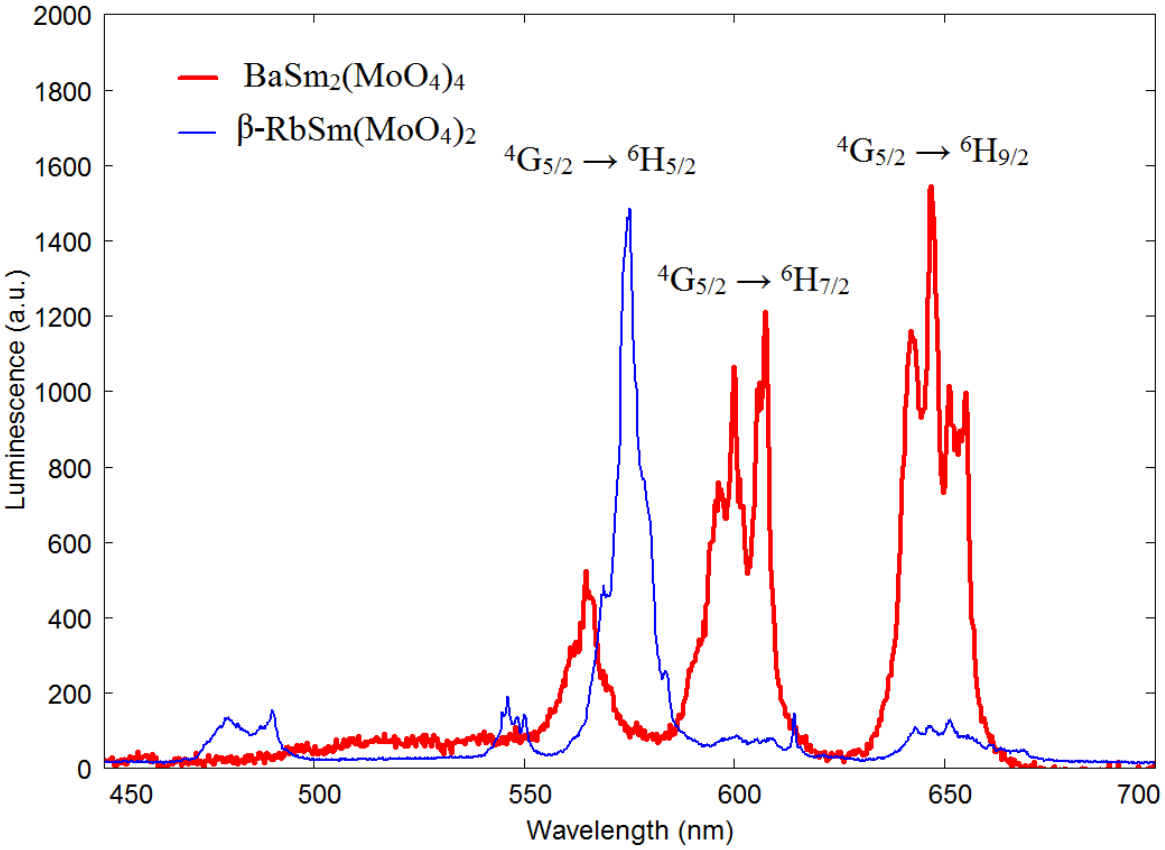
BaSm2(MoO4)4
β-RbSm(MoO4)2
4G5/2 → 6H5/2
4G5/2 → 6H7/2
4G5/2 → 6H9/2
Luminescence (a.u.)
Wavelength (nm)
0
200
400
600
800
1000
1200
1400
1600
1800
2000
450
500
550
600
650
700

Figure 6.

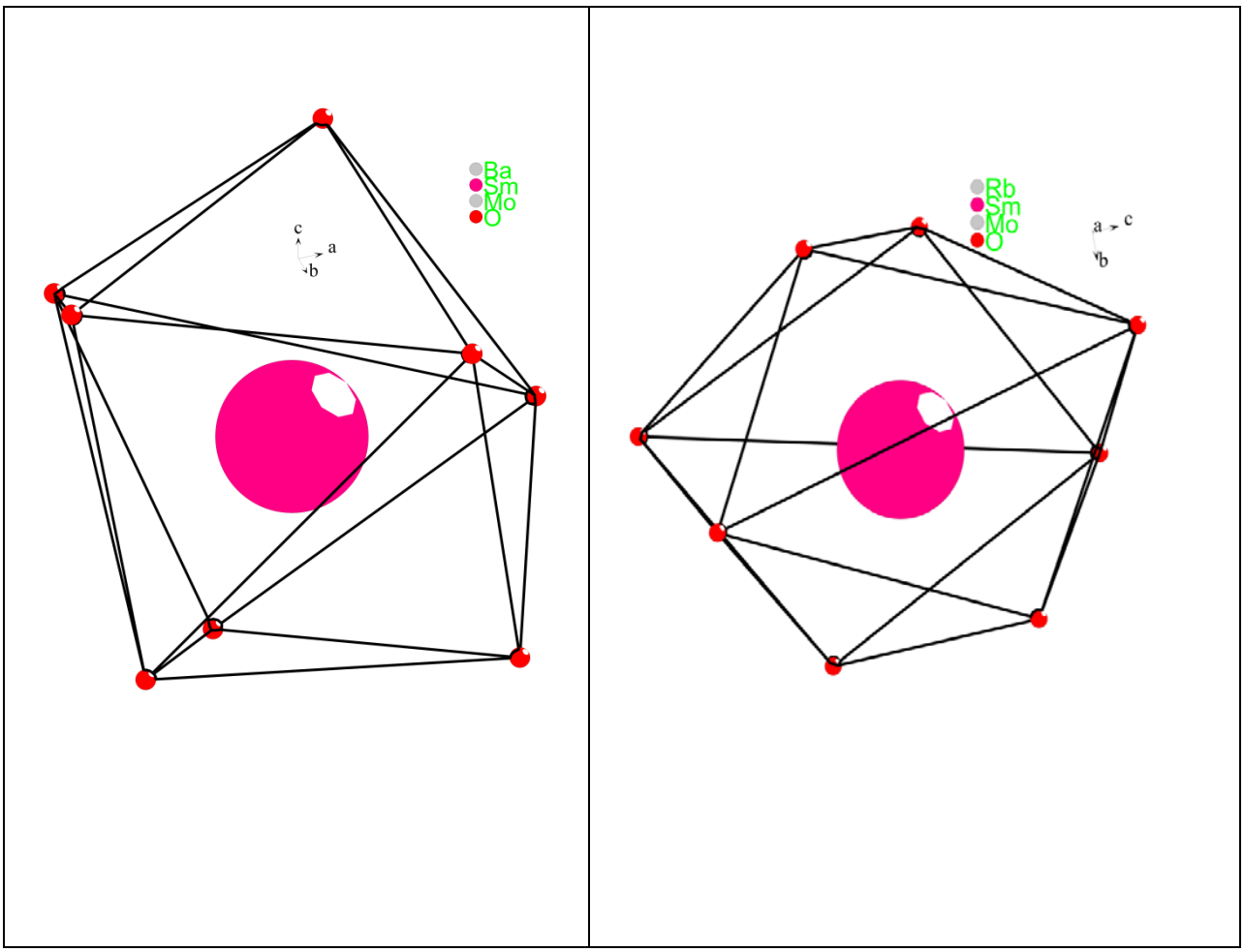

Figure 7.

Support

Crystal structure. luminescence and lattice dynamics of new monoclynic molybdate $BaSm_2(MoO_4)_4$

V.V.Atuchin[1,2,3,4,5], A.S. Aleksandrovsky[6,7], M.S. Molokeev[8,9], A.S. Krylov[10], A.S. Oreshonkov[10,11], Di Zhou[12,13]

[1]Laboratory of Optical Materials and Structures, Institute of Semiconductor Physics, SB RAS, Novosibirsk 630090, Russia

[2]Functional Electronics Laboratory, Tomsk State University, Tomsk 634050, Russia

[3]Laboratory of Semiconductor and Dielectric Materials, Novosibirsk State University, Novosibirsk 630090, Russia

[4]Institute of Chemistry, Tyumen State University, Tyumen 625003, Russia

[5]Laboratory of Single Crystal Growth, South Ural State University, Chelyabinsk 454080, Russia

[6]Laboratory of Coherent Optics, Kirensky Institute of Physics, Federal Research Center KSC SB RAS, Krasnoyarsk 660036, Russia

[7]Laboratory for Nonlinear Optics and Spectroscopy, Siberian Federal University, Krasnoyarsk 660041, Russia

[8]Laboratory of Crystal Physics, Kirensky Institute of Physics, SB RAS, Krasnoyarsk 660036, Russia

[9]Department of Physics, Far Eastern State Transport University, Khabarovsk 680021, Russia

[10]Laboratory of Molecular Spectroscopy, Kirensky Institute of Physics, Federal Research Center KSC SB RAS, Krasnoyarsk 660036, Russia

[11]Department of Photonics and Laser Technologies, Siberian Federal University, Krasnoyarsk 660079, Russia

[12]Electronic Materials Research Laboratory, Key Laboratory of the Ministry of Education & International Center for Dielectric Research, Xi'an Jiaotong University, Xi'an 710049, Shaanxi, China

[13]Materials Science and Engineering, University of Sheffield, Sheffield, S1 3JD, UK

Table 2. Fractional atomic coordinates and isotropic displacement parameters (Å^2) of $BaSm_2(MoO_4)_4$

	x	*y*	*z*	B_{iso}
Ba	0	0.4679 (2)	0.25	0.95 (7)
Sm	0.0034 (3)	0.3522 (1)	0.46735 (5)	0.43 (6)
Mo1	0.4949 (4)	0.2589 (2)	0.14992 (8)	0.47 (6)
Mo2	0.0104 (4)	0.0590 (2)	0.09179 (8)	0.55 (7)
O1	0.367 (3)	0.242 (1)	0.4316 (6)	1.1 (1)
O2	0.371 (3)	0.141 (1)	0.1763 (5)	1.1 (1)
O3	0.328 (3)	0.312 (1)	0.2823 (6)	1.1 (1)
O4	0.247 (3)	0.045 (1)	0.6078 (5)	1.1 (1)
O5	0.216 (3)	0.351 (1)	0.1364 (6)	1.1 (1)
O6	0.247 (3)	0.012 (1)	0.4661 (6)	1.1 (1)
O7	0.089 (3)	0.094 (1)	0.3298 (6)	1.1 (1)
O8	0.169 (2)	0.169 (1)	0.0483 (5)	1.1 (1)

Table 3. Main bond lengths (Å) of $BaSm_2(MoO_4)_4$

Ba—O2^{i}	2.70 (1)	Sm—O8^{iii}	2.52 (1)
Ba—O3	2.70 (1)	Sm—O8^{v}	2.41 (1)
Ba—O4^{ii}	3.04 (1)	Mo1—O1^{vi}	1.77 (1)
Ba—O5	2.92 (1)	Mo1—O2	1.73 (2)
Ba—O7^{i}	3.14 (1)	Mo1—O3^{vi}	1.73 (1)
Sm—O1	2.50 (1)	Mo1—O5	1.90 (1)
Sm—O1^{ii}	2.38 (1)	Mo2—O4^{vii}	1.85 (1)
Sm—O4^{ii}	2.38 (1)	Mo2—O6^{iii}	1.85 (1)
Sm—O5^{iii}	2.30 (1)	Mo2—O7^{iii}	1.68 (1)
Sm—O6^{ii}	2.51 (1)	Mo2—O8	1.85 (1)
Sm—O6^{iv}	2.45 (1)		

Symmetry codes: (i) -*x*+1/2, *y*+1/2, -*z*+1/2; (ii) -*x*+1/2, -*y*+1/2, -*z*+1; (iii) -*x*, *y*, -*z*+1/2; (iv) *x*-1/2, *y*+1/2, *z*; (v) *x*-1/2, -*y*+1/2, *z*+1/2; (vi) -*x*+1, *y*, -*z*+1/2

Table 1S. Parameters of the interatomic interaction potential

Interaction	λ, aJ/Å^2	ρ, Å
Ba – O	326.23	0.3876
Sm – O	300.75	0.3845
Mo1 – O1	411.59	0.4061
Mo1 – O2	419.19	0.4087
Mo1 – O3	403.99	0.4032
Mo1 – O5	395.07	0.3981
Mo1 – O*	408.27	0.4007
Mo2 – O4	388.67	0.3989
Mo2 – O6	413.51	0.4093
Mo2 – O7	414.75	0.4089
Mo2 – O8	404.95	0.4086
Mo2 – O*	402.51	0.4013
O – O	299.47	0.3853

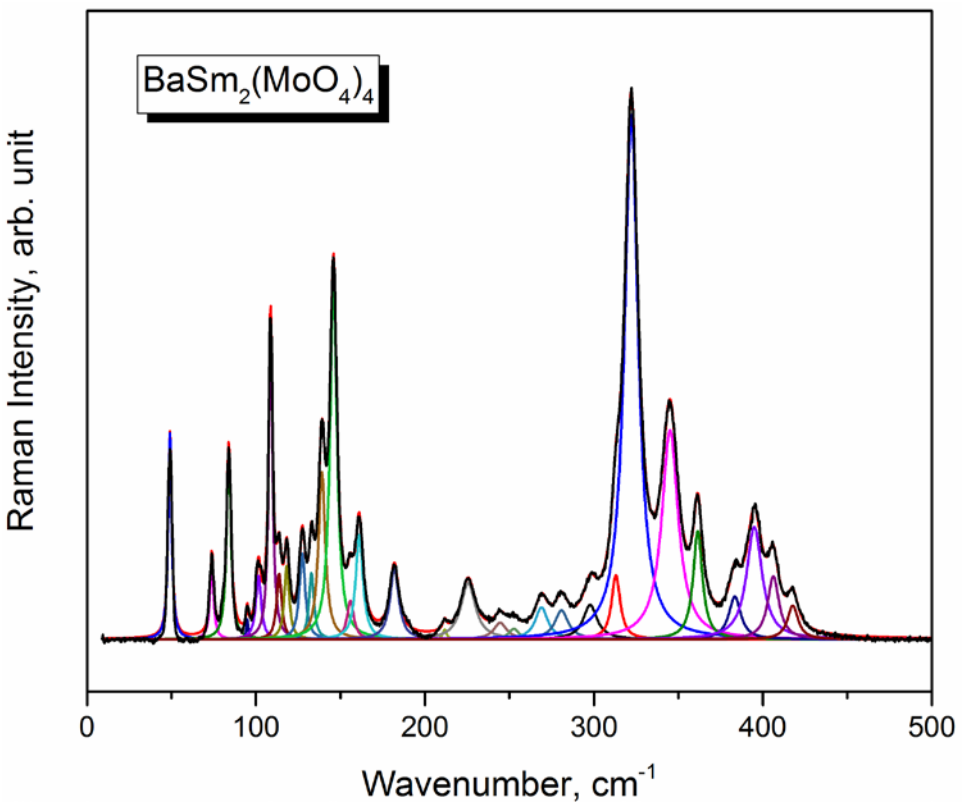

Fig. 1S. Raman spectrum decomposition over the low-wavenumber range.

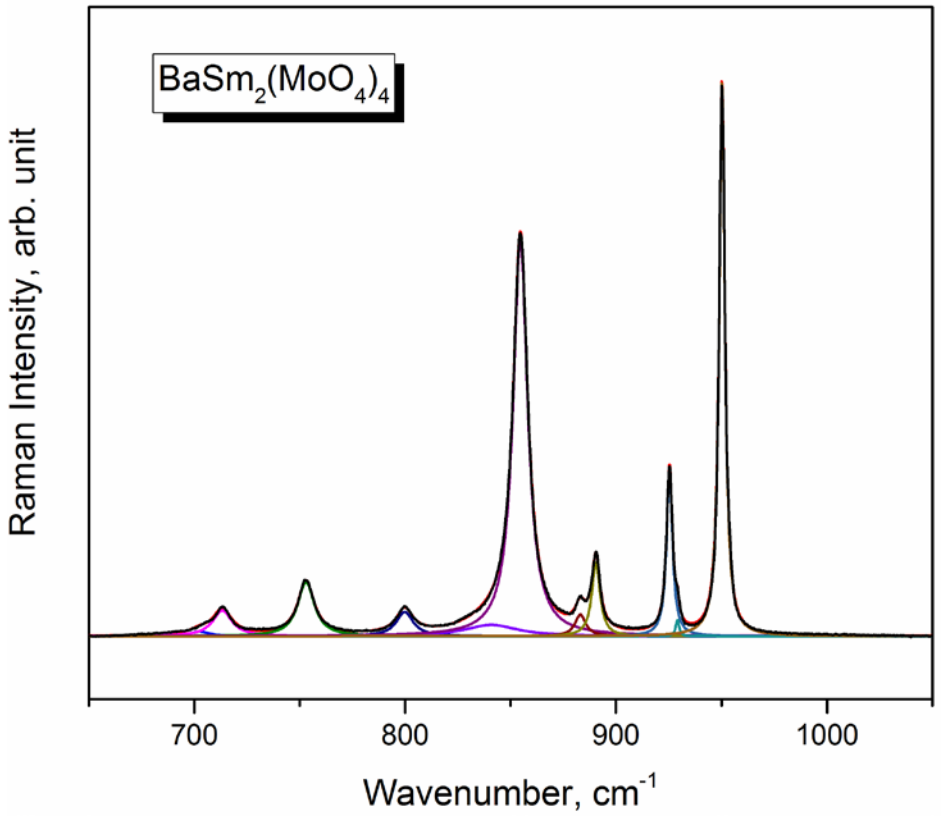

Fig. 2S. Raman spectrum decomposition over the high-wavenumber range.

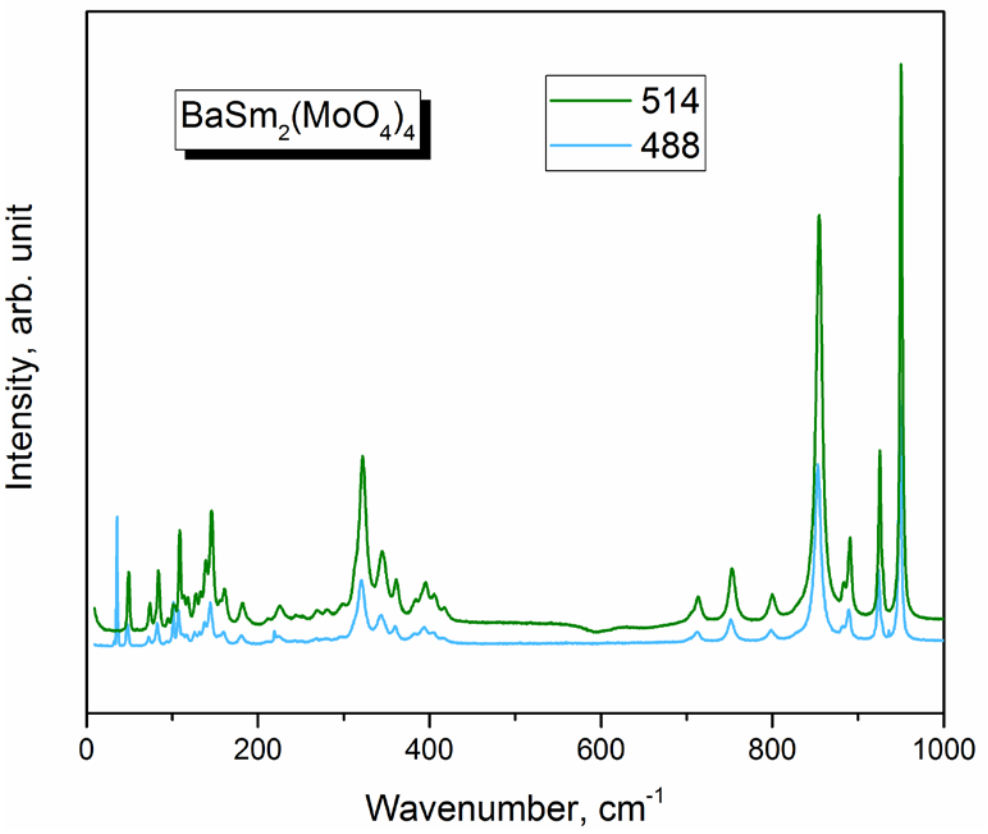

Fig. 3S. Raman spectrum recorded with excitation at 488 and 514.5 nm.